Identification of Drought Events in Major Basins of Africa from GRACE Total Water Storage and Modeled Products

Ayman M. Elameen, Shuanggen Jin, and Daniel Olago

Abstract

Terrestrial water storage (TWS) plays a vital role in climatological and hydrological processes. Most of the developed drought indices from the Gravity Recovery and Climate Experiment (GRACE) over Africa neglected the influencing roles of individual water storage components in calculating the drought index and thus may either underestimate or overestimate drought characteristics. In this paper, we proposed a Weighted Water Storage Deficit Index for drought assessment over the major river basins in Africa (i.e., Nile, Congo, Niger, Zambezi, and Orange) with accounting for the contribution of each TWS component on the drought signal. We coupled the GRACE data and WaterGAP Global Hydrology Model through utilizing the component contribution ratio as the weight. The results showed that water storage components demonstrated distinctly different contributions to TWS variability and thus drought signal response in onset and duration. The most severe droughts over the Nile, Congo, Niger, Zambezi, and Orange occurred in 2006, 2012, 2006, 2006, and 2003, respectively. The most prolonged drought of 84 months was observed over the Niger basin. This study suggests that considering the weight of individual components in the drought index provides more reasonable and realistic drought estimates over large basins in Africa from GRACE.

Introduction

Droughts have increased in frequency and severity due to climate change throughout the world's river basins in recent decades (Forootan *et al.* 2019). According to the sixth assessment report of the International Panel for Climate Change (IPCC), global temperatures have risen by ~1°C since industrialization, which may further amplify by 1.5°C between 2030 and 2050 as a result of human activities (IPCC 2018). As the population grows and water demand increases, droughts are triggered and aggravated by anthropogenic activities such as deforestation and the construction of dams (Schlosser *et al.* 2014; AghaKouchak 2015; Omer *et al.* 2020; Sarfo *et al.* 2022). To prioritize adaptation actions in global hot spots, it is essential to characterize droughts.

Although the continent has abundant water resources with meeting its ecological and agricultural needs, climatic extremes are becoming increasingly perilous, endangering the valuable water supply and millions of lives on the continent (Masih *et al.* 2014; IPCC 2022). Two of the biggest drought tragedies ever documented in history occurred in the Sahel region in 2007 and the Nile basin in 1984. These droughts caused the death of approximately 750 000 people (Vicente-Serrano *et al.* 2012). Future projections indicate that the probability of drought occurrence will increase across the entire African continent, leading to significant regional implications (Ahmadalipour and Moradkhani 2018; IPCC 2022). Additionally, excessive water demand may lead to the overuse of freshwater resources, which might result in disputes among water users during dry spells. This may increase the risk of hydro-political tension in Africa, as the Transboundary Rivers represent 64% of the entire region's landmass (United Nations Environment Program 2010). Monitoring the drought situation in Africa is crucial for prioritizing adaptations to avert water scarcity and disputes.

Long and uninterrupted in situ hydro-climatic observations are required for drought monitoring. Yet Africa's land-based observation network has been deteriorating with time, having only one-eighth of the minimum density required by the World Meteorological Organization and with only 22% of stations fully meeting the Global Climate Observing System requirements (Dobardzic *et al.* 2019). Due to the insufficiency of in situ data records in Africa, monitoring hydrological drought in the continent's basins has been limited (Ferreira *et al.* 2018). Additionally, a substantial financial and political commitment is required to record and share in situ observations, both of which are frequently missing. Remote sensing observations represent an alternative source to counter data deficiencies in many data-poor regions worldwide. Moreover, satellite-borne sensors have featured as an effective tool for tracking droughts, considering their capacity to offer regional-to-global coverage (Jiao *et al.* 2021).

Several remote sensing–based products have been used globally to assess and detect drought situations. Among these are Moderate Resolution Imaging Spectroradiometer (MODIS)–based evapotranspiration, soil moisture from Sentinel-1 and the Soil Moisture Active Passive radiometer, and the Normalized Difference Vegetation Index from Landsat (West *et al.* 2019; Modanesi *et al.* 2020). Although these measurements could deliver valuable information about agricultural and meteorological droughts, the task of assessing hydrological drought remains daunting (Papa *et al.* 2022) since they can capture only surface and shallow subsurface conditions. Also, it is problematic to evaluate droughts based only on surface measurements (e.g., precipitation and soil moisture), as the reduction of water from the deepest aquifers may continue even after the surface storage has dried up (Leblanc *et al.* 2009). After launching the Gravity Recovery and Climate Experiment (GRACE) satellite mission in 2002, the potential time-variable gravity measurement offered an integrated perspective for drought monitoring since it can capture vertically integrated terrestrial water storage (TWS)

Ayman M. Elameen is with the School of Remote Sensing and Geomatics Engineering, Nanjing University of Information Science and Technology, Nanjing 210044, China.

Shuanggen Jin is with the School of Remote Sensing and Geomatics Engineering, Nanjing University of Information Science and Technology, Nanjing 210044, China; the School of Surveying and Land Information Engineering, Henan Polytechnic University, Jiaozuo 454000, China; and Shanghai Astronomical Observatory, Chinese Academy of Science, Shanghai 200030, China (sgjin@nuist.edu.cn; sg.jin@yahoo.com).

Daniel Olago is with the Department of Earth and Climate Sciences, University of Nairobi, Nairobi 00100, Kenya..

Contributed by Dongdong Wang, June 1, 2022 (sent for review September 14, 2022; reviewed by Alper Yilmaz, Vagner Goncalves Ferreira,).

Photogrammetric Engineering & Remote Sensing
Vol. 89, No. 4, April 2023, pp. 221–232.
0099-1112/22/221–232

doi: 10.14358/PERS.22-00092R2

changes (i.e., from the top surface water to the deepest groundwater) (Ndehedehe *et al.* 2018).

The unique potential of GRACE measurements offered hydrologists a new dimension to develop new GRACE-based drought indices (Hassan and Jin 2014; Jin and Zhang 2016). Therefore, numerous studies have applied GRACE-based indicators for drought analysis and monitoring. For example, Kumar *et al.* (2021) evaluated the drought severity over the Godavari basin using the GRACE Combined Climatologic Deviation Index. Liu *et al.* (2020) proposed a GRACE-based Drought Severity Index and assessed the drought variations for China's large basins. Khorrami and Gunduz (2021) proposed an Enhanced Water Storage Deficit Index to observe drought conditions in Turkey. Wu *et al.* (2021) characterized the drought over southwest China using the GRACE-derived Total Storage Deficit Index. Cui *et al.* (2021) developed a multiscale Standardized Terrestrial Index of water storage to assess the global hydrological droughts.

A number of studies have been performed to track droughts in Africa using different drought indices. Examples of earlier investigations and the indices used by different authors are listed in Table 1. The majority of used indices either originated from a single TWS component, such as surface water (precipitation) or were created primarily to take into account the total TWS components, including surface, soil, ground, snow, and canopy water. The influence role of the individual TWS components in drought index is not taken into account in these previous studies. Each water storage component is an essential hydrological variable to comprehend drought occurrences, according to Lopez *et al.* (2020). Since the TWS-based drought indicator considers all components together, the primary problem is abstract. As a result, it is more reasonable to analyze these components separately since one of them (e.g., groundwater) could alleviate the drought impact. Therefore, this study aims to consider the role of individual TWS components and their relative contributions to drought index computing, which might lead to a more reasonable and realistic drought evaluations.

Answering the topic of how different water storage elements respond to drought conditions throughout Africa's major river basins is the main goal of this study. To do this, we used the Weighted Water Storage Deficit Index (WWSDI) (Wang *et al.* 2020), which was developed from the GRACE WSDI but also considered the influence of the individual TWS components to provide further reliable droughts assessment. We used the WWSDI to identify the critical drought characteristics (i.e., severity, intensity, and duration) over five Africa's major river basins (Nile, Congo, Niger, Zambezi, and Orange) (see Figure 1) during the 2003–2016 period. We further compared the analysis of WWSDI against the GRACE-based Water Storage Deficit Index (WSDI) and the commonly used indicators—the self-calibrated Palmer Drought Severity Index (scPDSI), the Standardized Precipitation Index, and the Standardized Precipitation Evapotranspiration Index—to assess its efficiency. The understudied river basins in this article represent the major sources of temporal fluctuations of hydrological masses across the continent. They lie between 32.6°S to 31.4°N and 11.5°W to 39.8°E and cover a broad range of different sizes, and climate zones vary from humid to semiarid. More details regarding these basins are provided in Table 2. Further details on the data sets, the methods used, and results are highlighted in subsequent sections.

Table 1. Different drought indices employed in previous studies.

River Basin	Drought Indices/Data Inputs	References
Nile	GRACE TWSD	Hasan *et al.* (2021)
	SPI, SPEI, SSI	Nigatu *et al.* (2021)
	MSDI	
	PDSI	
	GRACE WSDI	
	GRACE CCDI	
	GRACE GGDI	
Congo	SPI, SRI	Ndehedehe *et al.* (2019)
	SPI, GRACE TWS change, MERRA TWS change	Ndehedehe *et al.* (2017)
	SPEI, GRACE-TWS change	Ndehedehe *et al.* (2020)
Niger	De-seasoned GRACE TWS change	Ferreira *et al.* (2018)
	SPI, SPEI, SRI	Oguntunde *et al.* (2018)
	SPI, GRACE TWS change, MERRA TWS change	Ndehedehe *et al.* (2017)
Zambezi	GRACE WSD	Thomas *et al.* (2014)
	SPI, TSDI	Hulsman *et al.* (2021)
	WLDI	
Orange	SPI, SPEI	Abiodun *et al.* (2019)

CCDI = Combined Climatologic Deviation Index; GGDI = GRACE Groundwater Drought Index; GRACE = Gravity Recovery and Climate Experiment; MSDI = Precipitation and Soil Moisture Integrated Index; PDSI = Palmer Drought Severity Index; SPEI = Standardized Precipitation Evapotranspiration Index; SPI = Standardized Precipitation Index; SRI = Standardized Runoff Index; SSI = Soil Moisture Index; TSDI = Total Storage Deficit Index; TWSD = total water storage deficit; WLDI = Water-Level Deficit Index; WSD = water storage deficit; WSDI = Water Storage Deficit Index.

Table 2. Area, length, climate, and mean annual precipitation of river basins selected in this study.

River Basin	Area (10^5 km^2)	Length (km)	Climate	Mean Annual P (mm)	Elevation (m)
Nile	31.8	6700	Semiarid	678	726
Congo	37.5	4667	Humid	705	737
Niger	21.8	4200	Semiarid	1504	419
Zambezi	13.8	2650	Semiarid	975	1003
Orange	9.7	2300	Semiarid	359	270

Materials and Methods

Data Sets

In this section, we provide a brief introduction of the data used in this study. Table 3 provides a tentative summary.

Precipitation

The study of droughts requires a thorough grasp of precipitation. This study uses monthly precipitation of 0.25° × 0.25° from 2003 to 2016, acquired from the seventh version of the Tropical Rainfall Measurement Mission (TRMM 3B43) (Huffman *et al.*, 2007). Numerous studies (Ferreira *et al.* 2018; Abd-Elbaky and Jin 2019) have been conducted over Africa using this data set. Moreover, Awange *et al.* (2016) reported that TRMM was suitable for hydrometeorological applications over most parts of Africa.

Potential Evapotranspiration

The present study utilizes monthly potential evapotranspiration (PET) retrieved from the MOD16A2 sensor, publicly available worldwide at 8-day temporal resolutions and 500-m spatial resolution (Running *et al.* 2017). We select MODIS16A2 data sets due to their relatively lower magnitude of uncertainty and rather good performance over the region (Andam-Akorful *et al.* 2015; Mekonnen *et al.* 2022). MODIS16A2 PET data extraction was conducted using Google Earth Engine (GEE). The 8-day PET data were averagely weighted to obtain the monthly PET values for this study.

GRACE-Derived TWS Anomalies

GRACE measurements (Jin *et al.* 2011; Ndehedehe *et al.* 2020) provide useful information for hydrological studies since they offer a quantitative assessment of monthly variations of water in lakes, rivers, reservoirs, snow, soil, and aquifers. The present study employs the sixth release of the spherical harmonics coefficient solutions processed by the Center for Space Research (CSR) at the University of Texas at Austin (Zhang *et al.* 2018), to derive gridded terrestrial water storage anomaly (TWSA) data over the selected river basins from 2003 to 2016 at a spatial resolution of 1°.

The coefficients were processed by being truncated at degree and order 60. They were then filtered and destriped using a 400-km-radius Gaussian filter. The leakage reduction and averaging approach (Khaki *et al.* 2018) were used in this study to minimize the leakage error contributions over the understudied river basins. The missing months in the

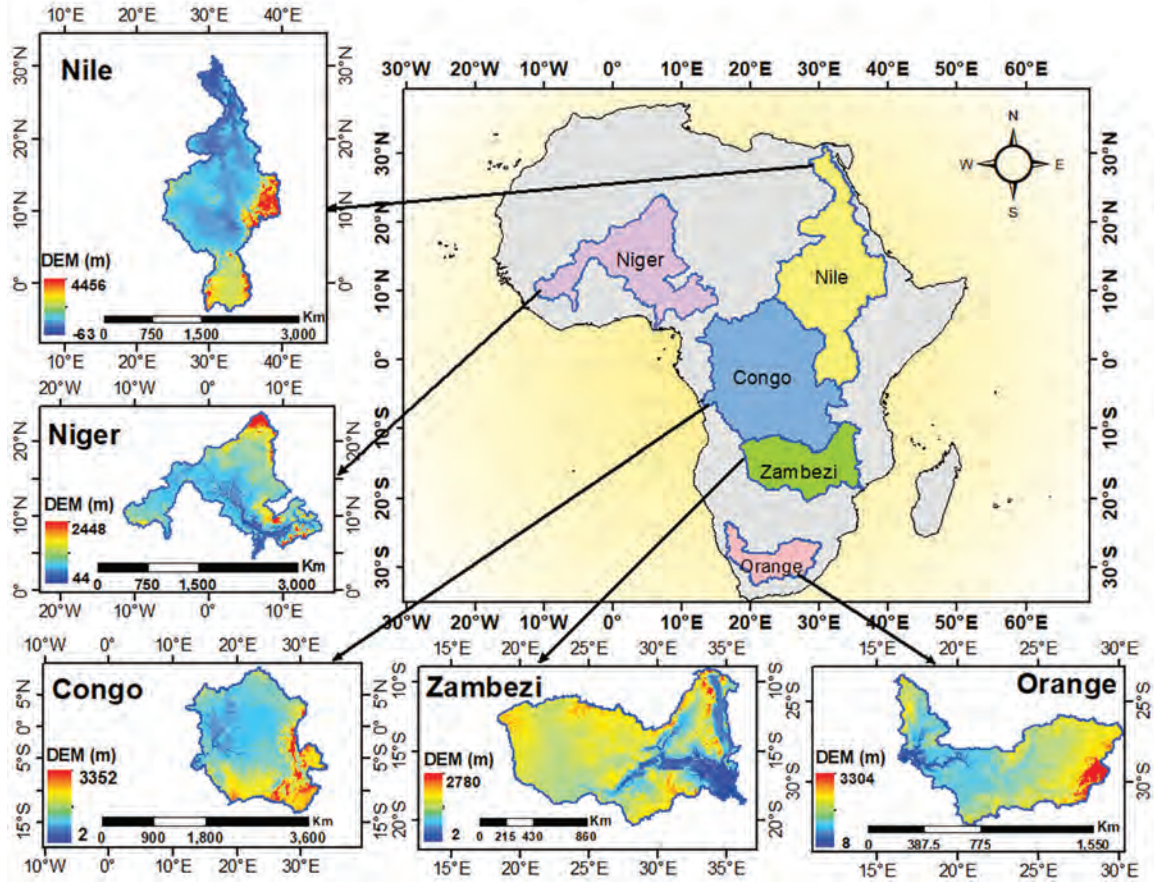

Figure 1. Map showing the location of river basins selected in this article and the elevations along the basins.

Table 3. Data sets used in this study.

Categories	Data/Model	Time Span	Spatial Resolution	Data Sources
GRACETWS	CSR-SH (RL06)	2003–2016	1°×1°	http://www2.csr.utexas.edu/grace/
Precipitation	TRMM	2003–2016	0.25°×0.25°	https://disc.gsfc.nasa.gov/datasets/TRMM_3B43_7
Surface water	WGHM	2003–2016	0.5°×0.5°	https://doi.pangaea.de/10.1594/PANGAEA.918447
Soil moisture	WGHM	2003–2016	0.5°×0.5°	https://doi.pangaea.de/10.1594/PANGAEA.918447
Snow water equivalent	WGHM	2003–2016	0.5°×0.5°	https://doi.pangaea.de/10.1594/PANGAEA.918447
Canopy water	WGHM	2003–2016	0.5°×0.5°	https://doi.pangaea.de/10.1594/PANGAEA.918447
Potential evaporation	MOD16A2	2003–2016	500 m	https://developers.google.com/earth-engine/datasets/catalog/MODIS_006_MOD16A2
scPDSI	CRU	2003–2016	0.5°×0.5°	https://crudata.uea.ac.uk/cru/data/drought/

CRU = Climate Research Unit; CSR = Center for Space Research; GRACE TWS = Gravity Recovery and Climate Experiment terrestrial water storage; scPDSI = self-calibrated Palmer Drought Severity Index; TRMM = Tropical Rainfall Measurement Mission; WGHM = WaterGAP Global Hydrology Model.

time series were filled using linear interpolation via averaging the prior and subsequent months (Yang *et al.* 2017).

scPDSI Gridded Data Sets

This study utilizes monthly scPDSI (Wells *et al.* 2004) time-series (v4.04) data sets for the period 2003–2016, with a spatial resolution of 0.5°. The data sets were collected from the Climate Research Unit (CRU) at the University of East Anglia, United Kingdom.

WaterGAP Global Hydrology Model

This study uses the WaterGAP Global Hydrology Model (WGHM) to separate the components of GRACE TWS data (i.e., surface water storage [SWS], soil moisture storage [SMS], groundwater storage [GWS], snow water equivalent [SWE], and plant canopy water storage [CWS]). Given that the SWS and GWS are taken into account, the WaterGAP model has an advantage over the Global Land Data Assimilation System (GLDAS) (Huang *et al.* 2019). Moreover, climate fluctuations and anthropogenic influences on water availability are also considered (Wang *et al.* 2020). The recent model version (WaterGAP 2.2d) at a resolution of 0.5° is used in this study (Müller Schmied *et al.* 2021). The data are available from January 2000 to December 2016.

Methodology

Processing Standardized Drought Indices

Standardized indices are widely used to quantify droughts worldwide. We employ SPI, SPEI, and scPDSI to assess the effectiveness of WWSDI in characterizing drought events over the chosen basins for this study. SPI is a meteorological drought index that is based only on precipitation (Satish Kumar *et al.* 2021). To compute SPI, the monthly TRMM precipitation is normalized by utilizing an equal probability function. SPEI is an expansion of SPI, as it includes the influence of evapotranspiration on drought under changing environments. SPEI is computed by subtracting precipitation from potential evapotranspiration using climatic water balance. Hence, TRMM precipitation and MOD16 PET products were employed to calculate SPEI. It required long-term observations to reliably calculate SPI and SPEI; however, many studies, such as Sun *et al.* (2018), have successfully used the available GRACE term to characterize drought phenomena. Both indicators can be obtained at different timescales (1, 3, 6, 9, 12, and 24 months). However, each timescale reflects a distinct condition. For example, 1 month could indicate meteorological types of droughts, 3 months could reflect the soil moisture conditions, 6 months may indicate anomalies in land water storage, and 9 months could depict the agricultural droughts well. Hence, to provide a solid validation for WWSDI performance, the 6-month timescale was employed since it can effectively demonstrate the TWS deficit that was monitored by WWSDI (Sun *et al.* 2018; Wang *et al.* 2020). Another widely used meteorological drought index is the scPDSI, which is developed based on the Palmer Drought Severity Index (PDSI) using a physical water balance model. The scPDSI timescale is fixed unlike the two indices previously described.

Processing Components Estimation

As mentioned previously, TWSA is composed of the following:

$$\mathrm{TWSA} = \mathrm{GWSA} + \mathrm{SMSA} + \mathrm{SWEA} + \mathrm{SWSA} + \mathrm{CWSA} \tag{1}$$

In this study, TWSA is estimated from Grace, whereas soil moisture storage anomalies (SMSA), snow water equivalent anomalies (SWEA), surface water storage anomalies (SWSA), and canopy water storage anomalies (CWSA) are the anomalies of SMS, SWE, SWS, and CWS, deduced from the WGHM. Groundwater storage anomalies (GWSA) are estimated via subtracting TWSA from the WGHM-derived components in Equation 1. Note that the SWEA and CWSA have minimal contribution to TWSA over African basins. Thus, they are assumed to be negligible and not considered in groundwater storage anomalies computation, as indicated in Equation 1 (further description provided in "Results and Analysis"). SMSA and SWSA are expanded into the spherical harmonic coefficients, truncated to 60°, ordered, and filtered by Gaussian filter.

Component Contribution Ratio

We utilized the component contribution ratio (CCR) to determine the mean percentage contribution of a single water storage component to the temporal variability of the total TWS (Huang *et al.* 2019). CCR is calculated as the ratio of the mean absolute deviation (MAD) of a storage component to the total TWS variability (TV), as expressed by (Zhang *et al.* 2019)

$$\mathrm{CCR}_S = \frac{\mathrm{MAD}_S}{\mathrm{TV}} \tag{2}$$

where $\mathrm{MAD}_s = \frac{1}{N}\sum_{t}^{N} | S_t - \bar{S} |$, S denotes the single storage components, and TV is the total variability, calculated as summation of all components MAD_s ($\sum_{S}^{\text{Storages}} \mathrm{MAD}_S$).

Processing the WWSDI

In this study, in order to depict drought in the five large Africa's basins, we adopted the WWSDI developed by Wang *et al.* (2020). WWSD is based on WSD, which represents the difference between TWSA time series and the monthly means of TWSA values (Thomas *et al.* 2014) and is computed as

$$\mathrm{WSD}_{u,v} = \mathrm{TWSA}_{u,v} - \overline{\mathrm{TWSA}_v} \tag{3}$$

where $\mathrm{TWSA}_{u,v}$ is the value of TWSA time series for the *v*th month of the *u*th year and $\overline{\mathrm{TWSA}_v}$ is the mean value of the *v*th month of TWSA during the study period. A negative deviation represents storage deficits. Furthermore, three continuous negative months or longer is considered a drought event (Thomas *et al.* 2014). In order to make comparisons against SPI, SPEI, and scPDSI in this study, the WSD is normalized to WSDI by the zero-mean normalization method, based on the expression

$$\mathrm{WSDI} = \frac{\mathrm{WSD} - \mu}{\sigma} \tag{4}$$

where σ and μ indicate standard deviations and the mean of the WSD time series, respectively. In order to construct WWSD, we incorporated different TWS components (i.e., GWS, SWS, and SMS) to the drought index by weighting these components through their CCR using Equation 2. We subsequently calculated the water deficit for each component (i.e., groundwater storage deficit [GWSD], surface water storage deficit [SWSD], and soil moisture storage deficit [SMSD]) like the WSD. Thereafter, WWSD was generated by combining these water components' deficits after multiplying them by their respective weights,

$$\mathrm{WWSD} = \omega_1\mathrm{GWSD} + \omega_2\mathrm{SWSD} + \omega_3\mathrm{SMSD} \tag{5}$$

where ω_i (= 1, 2, 3) represent the derived weight from Equation 2. Finally, WWSDI is achieved by normalizing WWSD, as shown in Equation 4.

Results and Analysis

Distribution of Precipitation, Terrestrial Water Storage, and Its Components

The monthly averaged TWSA variation and its individual components other than precipitation over 14 years (from January 2003 to December 2016) are illustrated in Figure 2. A clear seasonal cycle as well as interannual variation in the amount of TWSA, GWSA, SMSA, SWSA, and precipitation are visible for all the basins. CWSA and SWEA variations were observed to be minimal over all the basins. Thus, the latter two components are not considered in the following analysis.

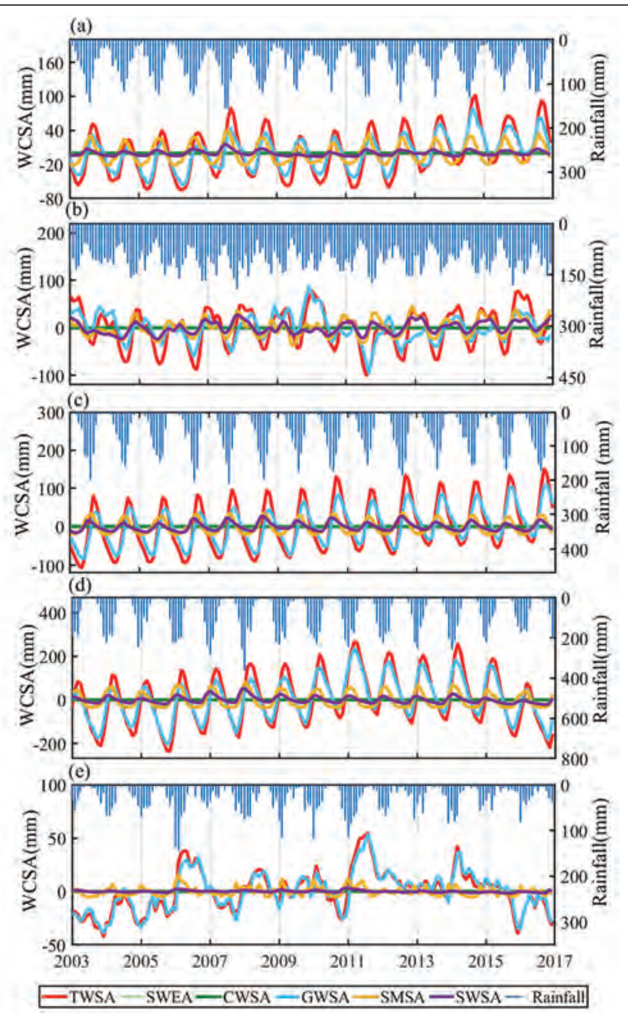

Figure 2. Time series of monthly precipitation, the terrestrial water storage anomaly (TWSA), and the terrestrial water components storage anomaly (WCSA) in the (a) Nile, (b) Congo, (c) Niger, (d) Zambezi, and (e) Orange river basins.

A comparison of precipitation and the TWSA seasonal cycle is shown in Table 4. It can be observed that both the Nile and the Niger basins followed broadly similar seasonal cycle variation since they have similar climatological/hydrological characteristics. Also, the Zambezi and Orange basins revealed similar pattern of the rainiest and driest months in terms of precipitation and TWSA.

It is clear from Figure 2 that a time lag exists between the peak of precipitation and TWSA as well as between the individual components of TWSA. Herein, the lag between TWSA, GWSA, SMSA, SWSA, and precipitation is further quantified via calculating the Pearson correlation coefficients among these storage components as well as the respective perception for different time lags (i.e., 0–12 months). Subsequently, the value of the maximum correlation coefficient between each two variables and the lags (numbers in brackets) corresponding to those maximum values are identified and shown in Figure 3.

The results from Figure 3 suggest a time lag of 0 to 2 months between TWS anomalies derived from GRACE and precipitation over the five basins. In general, the change in TWS was clearly noticeable in the season following the precipitation change over all basins (see Table 4). This result is consistent with the findings of Abd-Elbaky and Jin (2019) and Zhang *et al.* (2019). Concerning the lags between individual

Table 4. Wet and dry seasons of precipitation and terrestrial water storage anomalies (TWSA) over large African river basins.

	Wet Months		Dry Months	
River Basin	**Precipitation (mm)**	**TWSA (mm)**	**Precipitation (mm)**	**TWSA (mm)**
Nile	Jun–Aug (101.5)	Sep–Nov (48.3)	Dec–Feb (14.5)	Mar–May (−41.9)
Congo	Sep–Nov (154.4)	Dec–Feb (32.8)	Jun–Aug (7.9)	Sep–Nov (−47.2)
Niger	Jun–Aug (136)	Sep–Nov (75.7)	Dec–Feb (2.6)	Mar–May (−64.8)
Zambezi	Dec–Feb (204.6)	Mar–May(49.7)	Jun–Aug (2.8)	Sep–Nov (−188.6)
Orange	Dec–Feb (60.7)	Mar–May(6.45)	Jun–Aug (7.09)	Sep–Nov (−9.33)

Figure 3. Maximum Pearson correlation coefficients between monthly terrestrial water storage anomalies (TWSA), the individual components of TWSA, and precipitation in the (a) Nile, (b) Congo, (c) Niger, (d) Zambezi, and (e) Orange river basins. The numbers in brackets represent the corresponding lag months.

components of the TWSA and precipitation, the largest correlation coefficients were observed corresponding to 2 to 3 months of lag in terms of GWSA and 0 to 1 month in terms of SWSA and SMSA, respectively. The lags between GWSA, SMSA, and SWSA against precipitation can be arranged as GWSA > SMSA ≥ SWSA. These findings further supported the assertion of precipitation as a key driver of water storage, with immense control over the hydrological cycle in these basins.

In each basin, the lags between TWSA, individual components of TWSA, and precipitation are attributed mainly to each basin's peculiar geographical and climatological characteristics.

Figure 4 illustrates the calculated component contribution ratio (CCR) of GWSA, SMSA, and SWSA for the five major rivers in Africa. The results revealed that the highest contribution to total water storage variability over the five river basins was induced mainly by the GWS anomaly accounting (56%, 61%, 47%, 64%, and 78%), followed by SMSA (34%, 32%, 25%, 26%, and 18%) and SWSA (10%, 21%, 14%, 10%, and 4%) for the Nile, Congo, Niger, Zambezi, and Orange basins, respectively. Furthermore, SMSA and SWSA peaks and troughs are not necessarily coincident with the peaks and troughs of TWSA, as shown in Figures 2 and 3. This difference is attributed mainly to the different time lags between precipitation falling and the response of the single TWS components against the precipitation. These findings denote that different TWS components exhibit different amplitude, phase, and contributions to TWS change. This further confirms that different components contribute distinctly to TWS changes over the understudied basins. Given their unique contributions to the shift in TWS, it is natural to wonder whether these water components react differently to the incidence of drought over those basins. Further answers and analysis are provided in the following section.

Deficit of Terrestrial Water Components in the Major Basins of Africa

Figures 5 and 6 demonstrate the time series of the derived terrestrial water components storage deficit (WCSD) (including GWSD, SMSD, and SWSD) and terrestrial water storage deficit indices (WCSDI) (including GWSDI, SMSDI, and SWSDI) from January 2003 to December 2016 for the five major African basins. According to Figure 5, the overall correlation between GWSD and WSD for the five basins ranged from 0.91 to 0.99. SMSD and SWSD followed different patterns from that of GWSD during different periods in the time series. For example, over the Congo basin (Figure 5b), from January 2009 to January 2013, GWSD recorded a declining trend of −1.03 mm, whereas SMSD and SWSD exhibited rising trends of 0.3 mm and 0.15 mm, respectively.

To better understand the drought dynamics over the considered basins in this study, WCSD was also utilized as an indicator to identify drought events based on 3 months or more of continuous negative deficits (from January 2003 to December 2016), as shown in Figure 7. The results clearly show that different WCSD indicators detected varied onset, duration, and drought occurrences during the study period. For example, over the Nile basin (Figure 7a), groundwater storage deficit (GWSD) exhibited six drought events, whereas SMSD and SWSD exhibited 12 and 7 events, respectively, between January 2003 and December 2016. Moreover, a noticeable prolonged drought state in terms of groundwater storage (GWSD) was observed from January 2003 to February 2007, January 2003 to December 2009, January 2003 to July 2008, and January 2003 to January 2006 over the Nile, Niger, Zambezi, and Orange basins, respectively, separated by nearly one wetting month. The drought trends depicted from (Figure 7a, 7c, 7d, and 7e) are consistent with GWSDI (Figure 6a, 6c, 6d, and 6e). The late response of GWS to recharge from SWS and/or the increased groundwater withdrawal can support this finding. Furthermore, the Niger basin had the most prolonged GWS drought state among all the basins recording 7 years. Previous work by Ferreira *et al.* (2018) on a water storage (TWS) drought signal over West Africa (including the Niger basin) found a long drier period between 2003 and 2008. These findings are consistent with the results presented in this study. According to the analysis of the 2003–2008 period presented in this article, the water storage (TWS) based drought trend is related to groundwater storage, where most of the TWS (i.e., 61%) in the Niger basin is induced mainly by GWS (Figures 4 and 7c). Ferreira *et al.* (2018) reported that

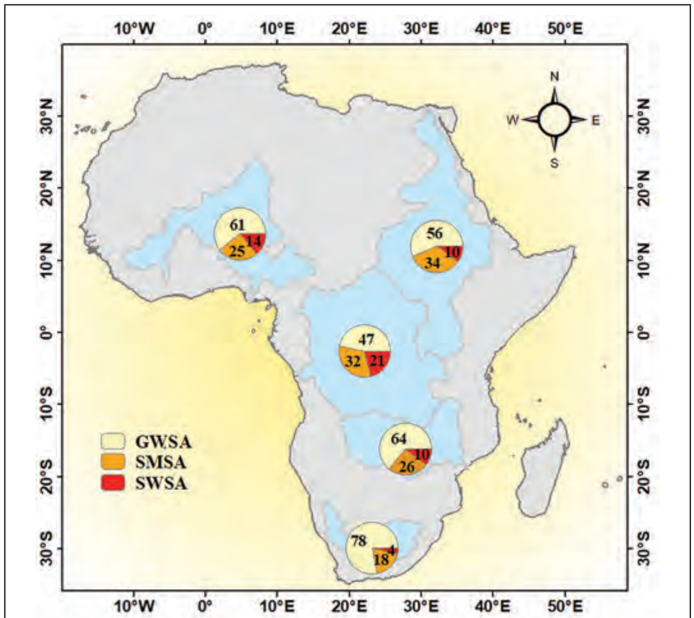

Figure 4. Component contribution ratios of groundwater storage anomalies (GWSA), soil moisture storage anomalies (SMSA), and surface water storage anomalies (SWSA) to the total water storage anomalies (TWSA) in the major river basins of Africa.

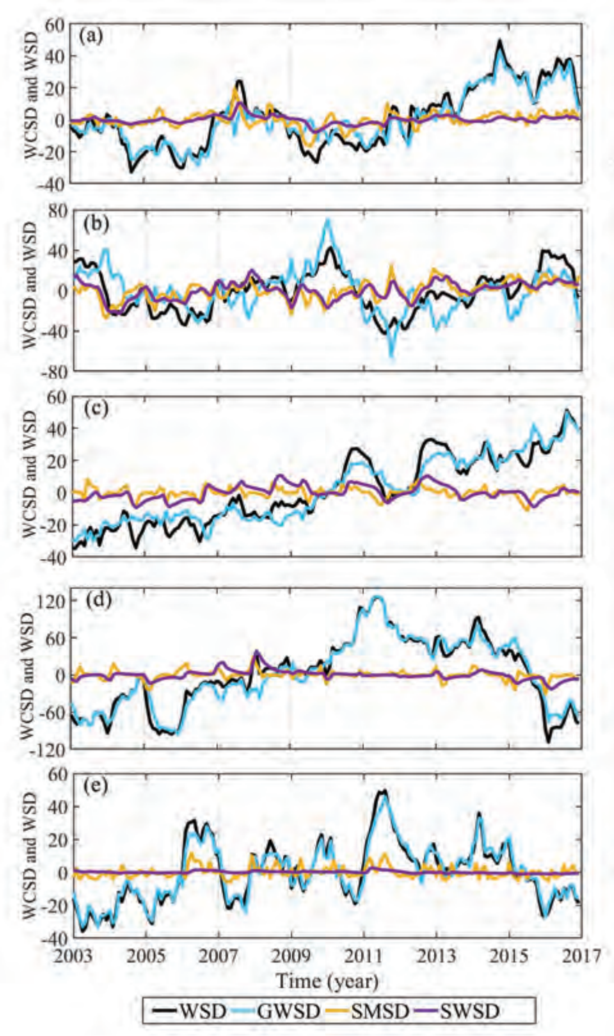

Figure 5. Time series of water storage deficit (WSD) and water components storage deficit (WCSD) in the (a) Nile, (b) Congo, (c) Niger, (d) Zambezi, and (e) Orange river basins.

the rainfall increasing trend between 2003 and 2008 over West Africa is associated with a drought period. They attributed this to the unsustainable influencing of rainfall recovery to the water-storage increase across West Africa, in the early 2000s. Consequently, the occurrence of the long GWS drought state in the Niger basin may be attributed to the minimal or late influences of surface water on the groundwater storage in the early 2000s.

The results also demonstrate that SWSD and SWSDI over the Orange basin (Figures 6e and 7e) exhibited a long drier period from March 2013 to December 2016 except for February and June 2013. This finding is in line with an early study conducted over the South African drying signal (Munday and Washington 2019). The latter linked the decline in precipitation with local surface temperature change since increased subsidence is linked to clearer skies and higher net solar radiation. Also, the reduction in precipitation magnitude is correlated to the changing patterns of tropical sea surface temperatures. Furthermore, the exceeding demand for surface water may cause the surface water shortage, where the water of the Orange basin is heavily utilized, and most of the riparian states rely on the Orange basin's water resources for commercial crop irrigation; in addition, 29 dams are operated over the river (Mgquba and Majozi 2020), which may cause large water abstractions.

The results acquired from WCSD and WCSDI analysis concluded that different water components responded differently to drought events over the basins in this study. Thus, these parameters can be considered for a more realistic and reliable drought evaluation over the major African basins.

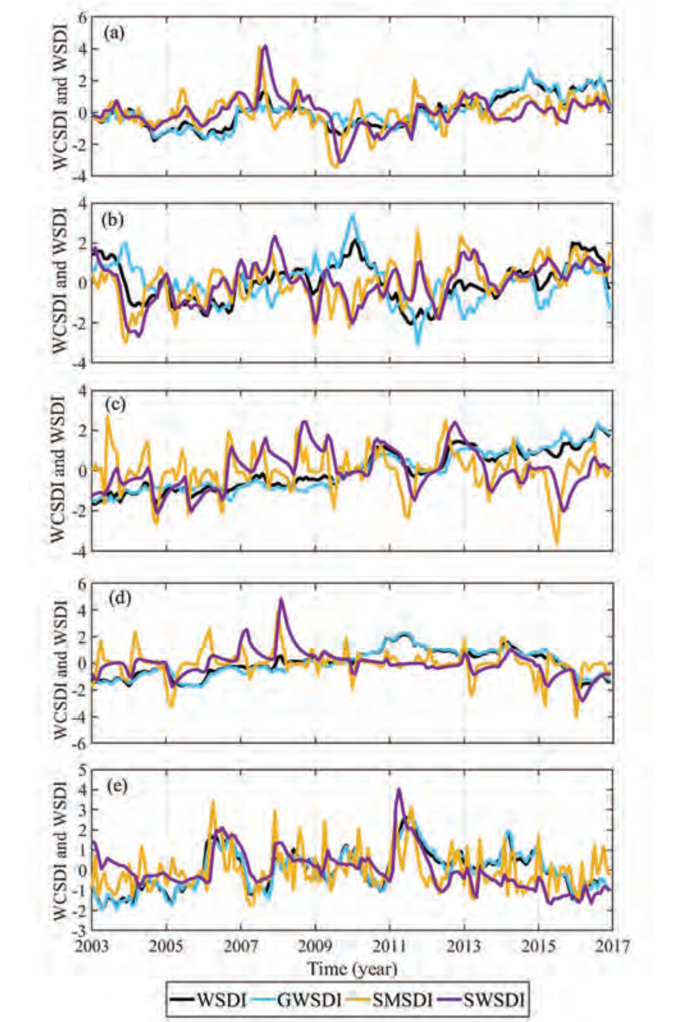

Figure 6. Time series of water storage deficit index (WSDI) and water components storage deficit index (WCSDI) in the (a) Nile, (b) Congo, (c) Niger, (d) Zambezi, and (e) Orange river basins.

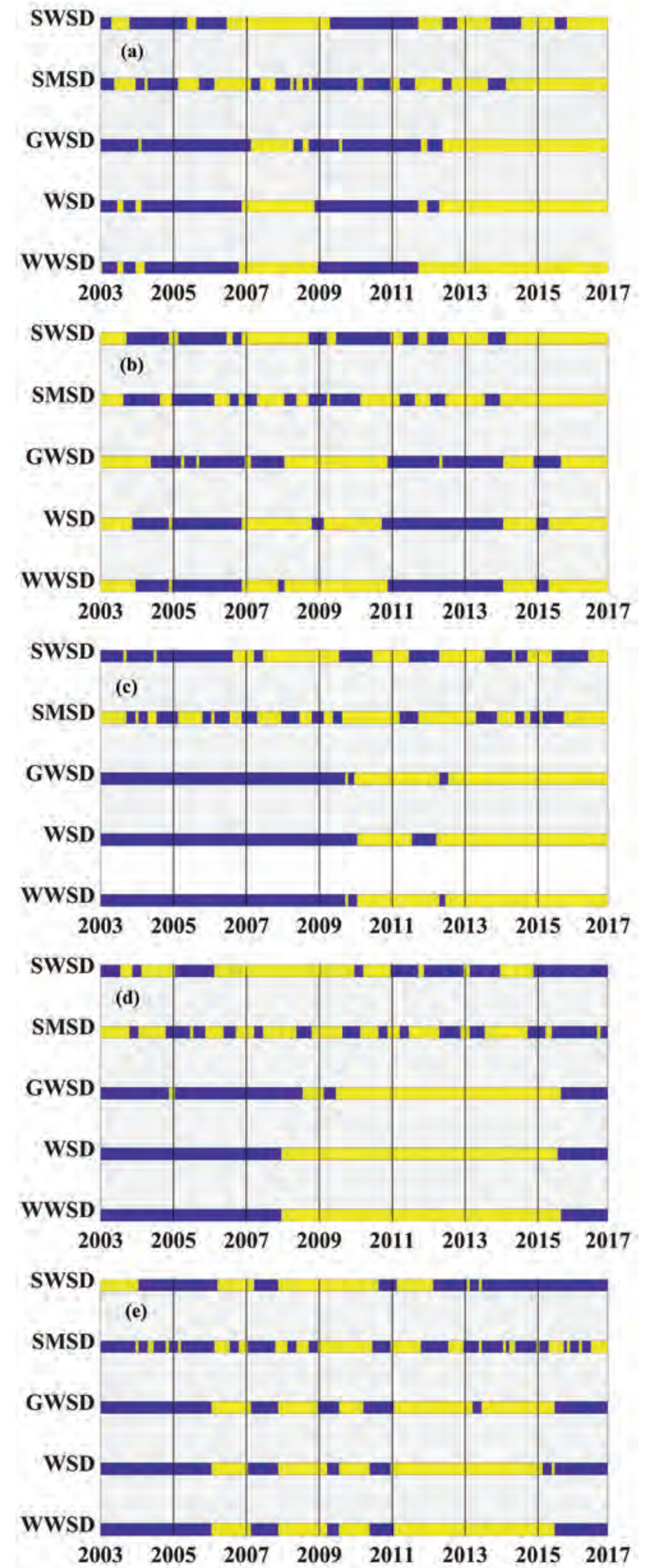

Figure 7. Temporal extents of identified drought events based on water storage deficit (WSD), water components storage deficit (WCSD), and weighted water storage deficit (WWSD) in the (a) Nile, (b) Congo, (c) Niger, (d) Zambezi, and (e) Orange river basins. The yellow values denote wet month, while the dark blue values represent drought month.

Evaluation of WWSD Relative to WSD

As previously shown, different water components play different roles in response to drought events over the basins in the study. The findings of this article have implications for how to provide a more realistic drought evaluation considering the individual TWS components and their relative contributions to the drought index. Therefore, to further demonstrate the rationality behind utilizing WWSD in this study, the performance of WWSD and WSD in terms of drought events identification has been assessed an is shown in Figure 7. Despite both indicators appearing to behave similarly, the data show some discrepancies in the observed onset and drought duration between WWSD and WSD. For example, in the Nile basin (Figure 7a), WWSD recorded one drought between April 2004 and October 2006, whereas WSD monitored the drought from March 2004 to November 2006. In the Congo basin (Figure 7b), WSD detected a drought event from November 2008 to January 2009; however, WWSD failed to identify this event. This result indicates that WWSD has varied sensitivity to drought events compared to WSD. These discrepancies, however, are explained by the weight given to a single TWS component in the WWSD. In conclusion, these findings suggest that accounting the influencing roles of these components storage in drought index are expected to provide more accurate drought characteristics estimation over major basins in Africa.

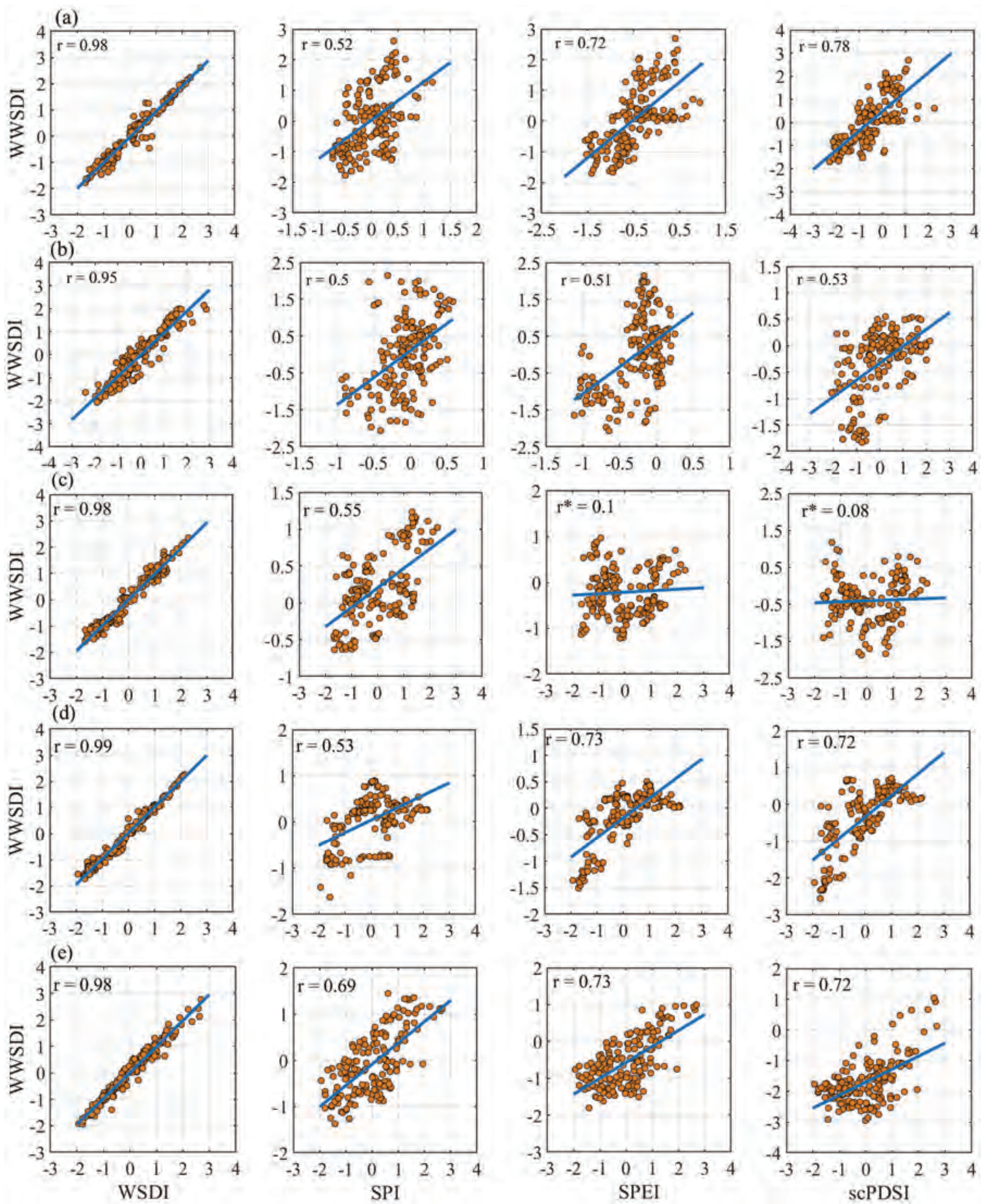

Figure 8. Scatterplots of correlation between the Weighted Water Storage Deficit Index (WWSDI) and Water Storage Deficit Index (WSDI), the Standardized Precipitation Index (SPI), the Standardized Precipitation Evapotranspiration Index (SPEI), and the self-calibrated Palmer Drought Severity Index (scPDSI) for the (a) Nile, (b) Congo, (c) Niger, (d) the Zambezi, and (e) Orange river basins. An asterisk indicates that the correlation is not significant.

WWSDI Identification of Droughts

In this study, the efficacy of WWSDI was identified by making comparisons with WSDI and other commonly used drought indices (i.e., SPI, SPEI, and scPDSI). The scatterplots in Figure 8 represent the correlation between WWSDI and WSDI, SPI, SPEI, and scPDSI over the five African river basins.

High positive correlations between WWSDI and WSDI are observed over the Nile, Congo, Niger, Zambezi, and Orange basins estimated at 0.98, 0.95, 0.98, 0.99, and 0.98, respectively. This strong relation between WWSDI and WSDI is due to their high sensitivity to GRACE TWS and the inclusion of TWS in their calculation procedures. However, the differences in correlation are attributed to the consideration of the weight of a single TWS component in WWSDI. WSDI is based on a single variable (GRACE TWSA); on the other hand, WWSDI is based on combining the TWS estimation from GRACE and WGHM using the CCR of individual TWS compartments as the weight. However, despite the fact that WWSDI and WSDI operate quite similarly, there is a distinction, as discussed in the previous section.

When comparing the WWSDI with other commonly used drought indices, we discovered that WWSDI is significantly correlated with SPI at a 0.05 significance level. The highest positive correlation ($r = 0.69$) between the two indices was observed in the Orange basin, while the lowest was detected in the Congo basin. WWSDI exhibited a significant correlation with the SPEI and scPDSI in the Nile, Congo, Zambezi, and Orange basins but a weak correlation in the Niger basin (Figure 8c).

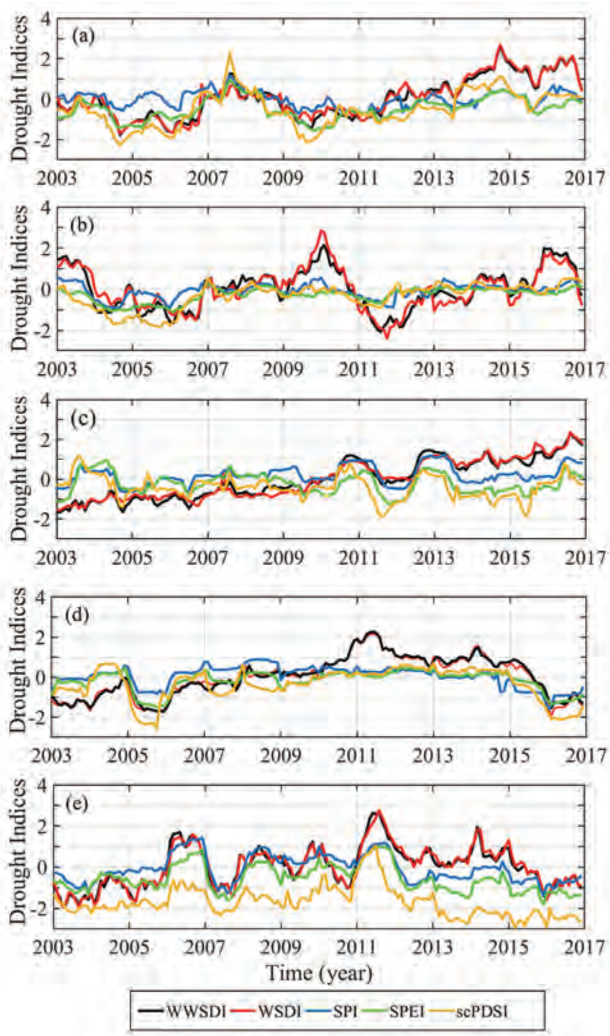

Figure 9. Time series of the Weighted Water Storage Deficit Index (WWSDI), the Water Storage Deficit Index (WSDI), the Standardized Precipitation Index (SPI), the Standardized Precipitation Evapotranspiration Index (SPEI), and the self-calibrated Palmer Drought Severity Index (scPDSI) for the (a) Nile, (b) Congo, (c) Niger, (d) Zambezi, and (e) Orange river basins.

In order to undertake a more thorough study, we further evaluated the temporal trends of these time series in Figure 9 in light of the fact that the association between the WWSDI and SPI, SPEI, and scPDSI was strongest in some situations while being less in others. As shown in Figure 9, the performance of WWSDI and its response to climate change correspond to the peaks and troughs of SPI, SPEI, and scPDSI over most basins. For example, all indicators showed that the biggest troughs occurred in the Orange basin in 2003 and across the Nile and Zambezi basins in 2006. However, in several cases, WWSDI was not fitting well with SPI, SPEI, and scPDSI; for example, the drought identified by WWSDI in 2004 over the Niger basin was not detected by SPI, SPEI, and scPDSI. The variations in relationships among SPI, SPEI, scPDSI, and WWSDI are most likely due to the differences in hydrological components and algorithms. For example, the high correlation between the scPDSI against WWSDI in the Nile basin reflects the significant influence of soil moisture on the TWS. Some recent studies also reported the significant correlation between soil moisture and TWS over the Nile basin (e.g., Abd-Elbaky and Jin 2019). In contrast, the weak correlation of SPEI and scPDSI with WWSDI in the Niger basin reveals that TWS was not much affected by evapotranspiration and soil moisture. In this context, the Niger basin was previously characterized as having a long-term high reduction in water storage between 2002 and 2008 (Ferreira *et al.* 2018), which corroborates our findings (Figure 7c). Thus, the availability of the stored water was less in the Niger basin, which affects the weak correlation of WWSDI against SPEI and scPDSI. Overall, WWSDI showed a good consistency with SPI, SPEI, and scPDSI in drought monitoring over most of the basins, which verifies the reliability of WWSDI in this study.

Analysis of Droughts in the Major Basins of Africa

Figure 10 displays the WWSDI-obtained droughts events for the major African basins from January 2003 to December 2016. Table 5 represents the magnitude, intensity, and duration characteristics of WWSDI for all the basins. The magnitude is calculated as accumulated WWSDI, and the intensity is calculated as the ratio of magnitude to duration (i.e., magnitude/duration) (Zargar *et al.* 2011; Wang *et al.* 2020).

Four drought events were detected in the Nile basin for 73 months during 2003, 2004–2006, and 2009–2011. In addition, two wet events occurred during 2006–2008 and 2011–2016; however, wet events became frequent after 2011. The most severe droughts (intensity of −1.15) occurred during 2004–2006 period, which is in line with the conclusions of previous studies conducted on the Nile basin (Hasan *et al.* 2021; Nigatu *et al.* 2021). The second and third severe drought events that took place during the 2009–2011 and 2003 regimes are consistent with the findings of Nigatu *et al.* (2021). However, in the current study, the results indicate that the identified drought episodes using WWSDI exhibited less magnitude than what was reported by Nigatu *et al.* (2021), who used WSDI. Moreover, the current study witnessed more recovery periods, particularly during the 2014–2016 period, than that of Nigatu *et al.* (2021). These differences can be attributed to the GRACE data period and to the fact that treating the weight of different TWS components equally may overestimate the severity and duration of drought conditions in the Nile basin. In the Congo basin, six drought events over 79 months were observed during the 2004, 2005–2006, 2007, 2010–2012, 2013–2014, and 2015 periods; in addition, five wet events were identified during the 2003–2004, 2008, 2009–2010, 2014, and 2015–2016 periods. The years 2010–2012 exhibited the highest frequency of droughts (with an intensity of −1.23). Our findings are in line with those of who observed the big drought occurrences that occurred over the Congo basin in 2005, 2006, and 2012. In the Niger basin, two prolonged drought episodes for 84 months were detected during 2003–2007 and 2007–2009; in addition, two significant wet events were observed between 2010–2011 and 2012–2016. However, after the 2009 period, there was a transition from dry to wet conditions. The severest drought event (intensity of −1.02) occurred during the 2003–2007 period, which is consistent with the findings of Ferreira *et al.* (2018), who carried out a study on the Niger basin. In the Zambezi basin, three drought events for 76 months were observed during the 2003–2004, 2005–2007, and 2015–2016 periods. Moreover, extended wet periods with water gain that began gradually in

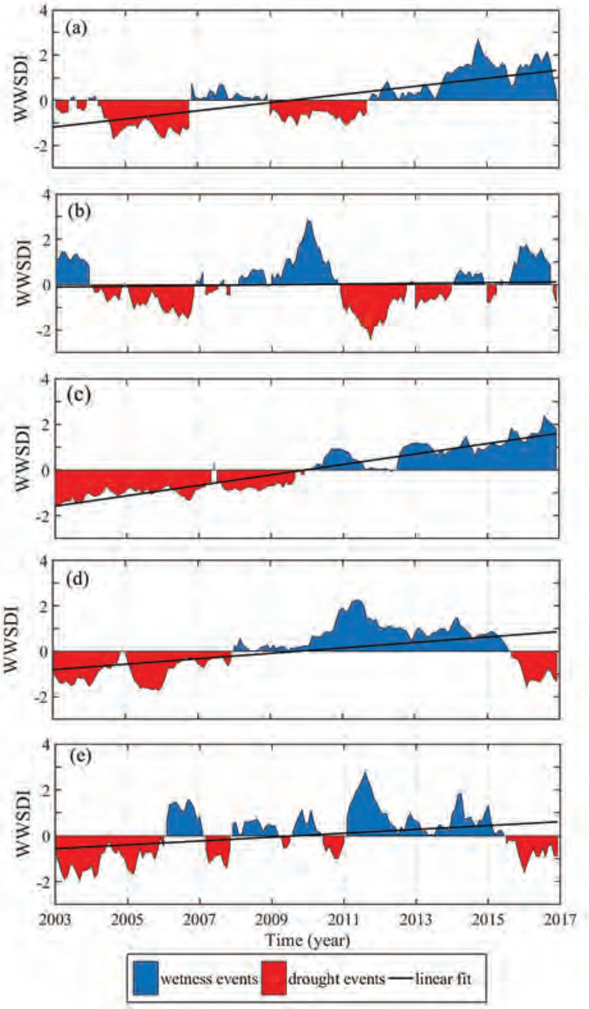

Figure 10. Drought events during 2003–2016 based on the Weighted Water Storage Deficit Index (WWSDI) for the (a) Nile, (b) Congo, (c) Niger, (d) Zambezi, and (e) Orange river basins.

Table 5. Drought characteristics in the major river basins in Africa identified by the Weighted Water Storage Deficit Index (WWSDI).

River Basin	No.	Period	Magnitude	Intensity	Duration
Nile	1	Feb 2003–Jun 2003	−2.39	−0.48	5
	2	Sep 2003–Dec 2003	−1.45	−0.36	4
	3	Apr 2004–Oct 2006	−35.78	−1.15	31
	4	Jan 2009–Sep 2011	−22.36	−0.68	33
Congo	1	Jan 2004–Nov 2004	−4.25	−0.39	11
	2	Jan 2005–Nov 2006	−24.85	−1.08	23
	3	Mar 2007–Jul 2007	−1.55	−0.31	5
	4	Dec 2010–Oct 2012	−28.40	−1.23	23
	5	Jan 2013–Jan 2014	−8.01	−0.62	13
	6	Jan 2015–Apr 2015	−2.38	−0.60	4
Niger	1	Jan 2003–May 2007	−54.01	−1.02	54
	2	Jul 2007– Dec 2009	−19.64	−0.65	30
Zambezi	1	Jan 2003– Dec 2004	−24.34	−1.02	24
	2	Jan 2005– Dec 2007	−28.62	−0.79	36
	3	Sep 2015– Dec 2016	−15.7	−0.98	16
Orange	1	Jan 2003–Jan 2006	−40.07	−1.08	37
	2	Mar 2007–Nov 2007	−8.50	−0.95	9
	3	Apr 2009–Jul 2009	−1.30	−0.32	4
	4	Jun 2010–Jan 2011	−5.05	−0.63	8
	5	Jul 2015– Dec 2016	−12.89	−0.72	18

2008 and greatly escalated from 2010 until the second half of 2015 were found. The severest drought event (intensity of −1.02) occurred during the 2003–2004 period. In their retrospective analysis of the Zambezi basin, Hulsman *et al.* (2021) equally confirmed that drought events occurred in the 2003–2004, 2005–2007, and 2015–2016 periods. In the Orange basin, five drought events over a total of 76 months were identified during the 2003–2006, 2007, 2009, 2010–2011, and 2015–2016 periods. In addition, four wet events were observed during the 2006, 2007–2008, 2009–2010, and 2011–2015 periods. The severest drought event (intensity of −1.08) occurred during 2003–2006. Additionally, the identified drought events over the region in 2004, 2005, 2007, 2011, and 2013 are in agreement with the findings of Masih *et al.* (2014).

The deviations in our drought evaluation results, along with those of previous studies, could be attributed to the period of the data sets and the utilized index method (WWSD). Our results indicated long-term drought occurrence from 2003 to 2006 over the Nile basin, from 2003 to 2009 over the Niger basin, and from 2003 to 2008 over the Zambezi basin, with the inclusion of few wetting months. This article's findings confirmed a general wetting tendency for the Nile, Niger, Zambezi, and Orange basins. Also, a mild trend (close to 0 mm) over the Congo basin was observed. The onset of the drought recovery period was consistent with the precipitation trends over the five river basins. However, considering the impacts of temperature increases, Africa's vulnerability to large-scale droughts may continue to increase (Ahmadalipour and Moradkhani 2018). The weather circulations in Africa have also been strongly influenced by large-scale atmospheric modes, such as the Indian Ocean Dipole (Anyah *et al.* 2018; Ni *et al.* 2018).

Discussion

Since GRACE observations can track changes in large-scale water storage, they are an essential tool in hydro-climatological investigations. Although established drought indices based on GRACE TWS (such as the WSDI and DSI) can identify vertically integrated water storage deficits, it can be challenging to estimate how much groundwater, surface water, or soil moisture deficits contribute to the overall water loss (Emerton *et al.* 2016). Thus, they reflect only integrated drought conditions, including groundwater drought. Furthermore, under the influence of climate change, the change characteristics (e.g., magnitude, variability, and duration) of each component are quite different (Wang *et al.* 2022). As a result, rather than evaluating all components as a whole, it is required to study the influence of each component separately in order to better comprehend the effects of climate change. In this study, a comprehensive drought index (WWSDI) was applied to evaluate drought events over the five large basins in Africa. The constructed index considers the contribution of a single component of the TWS deficit (i.e., surface, soil moisture, and groundwater) to the total water loss. The WWSDI has been successfully applied to the Yangtze basin as a case study scenario (Wang *et al.* 2020). Contextually, we determined a significant consistency among WWSDI and GRACE WSDI, SPI, SPEI, and scPDSI over the five African basins. This may indicate solid evidence on the applicability and capability of WWSDI over the river basins of Africa. Our research revealed that various TWS components contributed differently to TWS change and responded differently to drought patterns across all basins. Findings also provides more granular and differentiated information that can help improve researchers' knowledge of the hydrological factors and how they contribute to the overall characteristics of drought occurrences in the region. Therefore, it is seen to be more trustworthy to develop drought indices from GRACE when considering water components individually and in a differently weighted manner.

In order to provide decision makers with unique information for planning and management, we have, for the first time, evaluated the deficiency change of TWS components and their reaction to climate change in vast African basins. However, until this study was conducted, analysis of water components in major African river basins was uncommon or rare. We acknowledge that some shortcomings and uncertainties remain existed in this study. First, the WWSDI time series is only 13 years, which is insufficient to conclude a robust finding from a climatic perspective; however, longer-term data (at least 30 years) are needed to determine the baseline of the occurrence and severity of water storage deficits (Liu *et al.* 2020). Furthermore, analysis of the severity of drought events based on three or more continuous negative values of WWSDI is not suitable for monitoring all drought events, particularly short-term drought (Wu *et al.* 2021). Additionally, it worth noting that using linear interpolation to fill the GRACE time series' missing values would also induce errors in drought estimation (Andam-Akorful *et al.* 2015; Sun *et al.* 2018). However, despite this approach being simple and widely used to handle missing data, other construction techniques, such as artificial neural networks, may provide more accurate data in the future (Ahmed *et al.* 2019).

Second, using WGHM outputs to separate water components from GRACE TWS might be subject to large uncertainty (Wang *et al.* 2020). Regarding the former, most of the existing global models, including WGHM and even local land surface models, are uncalibrated and unable to predict TWS components accurately, specifically groundwater storage (Hosseini-Moghari *et al.* 2020). This is mainly because of the intricate interplay between the aquifer and surface water hydrology. Nevertheless, Ferreira *et al.* (2020) introduced a unique reconstruction method that combines remotely sensed and modeled data in order to estimate the water compartments from TWS. This method may also improve the precision of WWSDI. Although GRACE measurements are found to be effective to monitor large- or global-scale drought, the resolutions of the GRACE observations are associated with certain limitations for use at the subbasin scale or submonthly time periods (Kumar *et al.* 2016; Li *et al.* 2019). Data assimilation techniques have been proposed in future studies to improve the limitations of the GRACE data and WWSDI estimates by assimilating the GRACE/FO observation into hydrological models. Thus, finer drought maps than of GRACE scale (around 150 000 km2 at midlatitudes) could be generated, which is crucial for accurate drought monitoring.

Conclusion

In recent decades, severe droughts have affected many river basins worldwide, causing environmental and social damage. Prioritizing adaptation measures requires drought evaluation over large river basins around the world. In this study, we generated the WWSDI based on combined TWS from GRACE and WGHM utilizing the CCR of each component as their weight to assess the occurrences of drought throughout the major African basins from January 2003 to December 2016. The main findings of the study are summarized as follows:

- Precipitation is the primary hydrologic input for the TWS change, and the distribution of both parameters showed a significant seasonal change in the five river basins.
- Regarding CCR, SMS and SWS rank the second and third, while GWS change ranks the first and accounts for 56%, 61%, 47%, 64%, and 78% of TWS change in the Nile, Congo, Niger, Zambezi, and Orange basins, respectively. These results showed that different water components contribute distinctly to TWS change over those basins.
- According to WCSD and WCSDI distribution, different water components play different roles in response to drought events in the basins. The WSDI, SPI, SPEI, and scPDSI are correlated significantly against WWSDI over the Nile, Congo, Zambezi, and Orange basins. In the Niger basin, SPI is significantly correlated with WWSDI. Overall, our findings indicate that the WWSDI can successfully detect drought events over major basins in Africa.
- Based on WWSDI, the most severe droughts occurred in 2006, 2012, 2006, 2006, and 2003 in the Nile, Congo, Niger, Zambezi, and Orange basins, respectively. A significant wetting tendency was detected over the Nile, Niger, Zambezi, and Orange basins, while a mild trend was observed in the Congo basin.

The study of this nature may be helpful to policymakers and managers with seeking to promote sustainable water resource management and development

Acknowledgments

This work was supported by Strategic Priority Research Program project of the Chinese Academy of Sciences (grant no. XDA23040100). We also thank Abubaker Omer, Mohamed Abdallah Ahmed Alriah, and Isaac Sarfo for discussions and suggestions.

References

Abd-Elbaky, M. and S. Jin. 2019. Hydrological mass variations in the Nile River Basin from GRACE and hydrological models. *Geodesy and Geodynamics* 10:430–438.

Abiodun, B. J.; N. Makhanya, B. Petja, A. A. Abatan, P. G. Oguntunde. 2019. Future projection of droughts over major river basins in Southern Africa at specific global warming levels. *Theoretical and Applied Climatology*., 137, 1785–1799.

AghaKouchak, A., D. Feldman, M. Hoerling, T. Huxman, J. Lund. 2015. Water and climate: Recognize anthropogenic drought. *Nature*., 524, 409–411.

Ahmadalipour, A. and H. Moradkhani. 2018. Multi-dimensional assessment of drought vulnerability in Africa: 1960–2100. *Science of the Total Environment* 644:520–535.

Ahmed, M., M. Sultan, T. Elbayoumi, and P. Tissot. 2019. Forecasting GRACE data over the africanwatersheds using artificial neural networks. *Remote Sensing* 11:1769.

Andam-Akorful, S. A., V. G. Ferreira, J. L. Awange, E. Forootan, and X. F. He. 2015. Multi-model and multi-sensor estimations of evapotranspiration over the Volta Basin, West Africa. *International Journal of Climatology* 35:3132–3145.

Anyah, R. O., E. Forootan, J. L. Awange, and M. Khaki. 2018. Understanding linkages between global climate indices and terrestrial water storage changes over Africa using GRACE products. *Science of the Total Environment* 635:1405–1416.

Awange, J. L.; V. G. Ferreira, E. Forootan, Khandu, S. A. Andam-Akorful, N. O. Agutu, X. F. He. 2016. Uncertainties in remotely sensed precipitation data over Africa. *International Journal of Climatology*., 36, 303–323.

Cui, A., J. Li, Q. Zhou, R. Zhu, H. Liu, G. Wu, Q. Li. 2021. Use of a multiscalar GRACE-based standardized terrestrial water storage index for assessing global hydrological droughts. *Journal of Hydrology*., 603, 126871.

Dobardzic, S., C. G. Dengel, A. M. Gomes, J. Hansen, M. Bernardi, M. Fujisawa, and J. Intsiful. 2019. *2019 State of Climate Services: Agriculture and Food Security*. Geneva: World Meteorological Organization.

Emerton, R. E., E. M. Stephens, F. Pappenberger, T. C. Pagano, A. H. Weerts, A. W. Wood, P. Salamon, J. D. Brown, N. Hjerdt, C. Donnelly, C. A. Baugh, and H. L. Cloke. 2016. Continental and global scale flood forecasting systems. *Wiley Interdisciplinary Reviews: Water* 3:391–418.

Ferreira, V., Z. Asiah, J. Xu, Z. Gong, and S. Andam-Akorful. 2018. Land water-storage variability over West Africa: Inferences from space-borne sensors. *Water* 10:380.

Ferreira, V. G., B. Yong, M. J. Tourian, C. E. Ndehedehe, Z. Shen, K. Seitz, and K. Dannouf. 2020. Characterization of the hydro-geological regime of Yangtze River basin using remotely-sensed and modeled products. *Science of the Total Environment* 718:137354.

Forootan, E., M. Khaki, M. Schumacher, V. Wulfmeyer, N. Mehrnegar, A.I.J.M. van Dijk, L. Brocca, S. Farzaneh, F. Akinluyi, G. Ramillien, C. K. Shum, J. Awange, and A. Mostafaie. 2019. Understanding the global hydrological droughts of 2003–2016 and their relationships with teleconnections. *Science of the Total Environment* 650:2587–2604.

Hasan, E., A. Tarhule, and P. E. Kirstetter. 2021. Twentieth and twenty-first century water storage changes in the Nile River Basin from GRACE/GRACE-FO and modeling. *Remote Sensing* 13:953.

Hassan, A. A. and S. Jin. 2014. Lake level change and total water discharge in East Africa Rift Valley from satellite-based observations. *Global and Planetary Change* 117:79–90.

Hosseini-Moghari, S. M., S. Araghinejad, K. Ebrahimi, Q. Tang, and A. AghaKouchak. 2020. Using GRACE satellite observations for separating meteorological variability from anthropogenic impacts on water availability. *Scientific Reports* 10:1–12.

Huang, Z., P.J.F. Yeh, Y. Pan, J. J. Jiao, H. Gong, X. Li, A. Güntner, Y. Zhu, C. Zhang, and L. Zheng. 2019. Detection of large-scale groundwater storage variability over the karstic regions in Southwest China. *Journal of Hydrology* 569:409–422.

Huffman, G. J., R. F. Adler, D. T. Bolvin, G. Gu, E. J. Nelkin, K. P. Bowman, Y. Hong, E. F. Stocker, and D. B. Wolff. 2007. The TRMM Multisatellite Precipitation Analysis (TMPA): Quasi-global, multiyear, combined-sensor precipitation estimates at fine scales. *Journal of Hydrometeorology* 8:38–55.

Hulsman, P., H.H.G. Savenije, and M. Hrachowitz. 2021. Satellite-based drought analysis in the Zambezi River Basin: Was the 2019 drought the most extreme in several decades as locally perceived? *Journal of Hydrology: Regional Studies* 34:100789.

IPCC. 2018. An IPCC special report on the impacts of global warming of 1.5 °C above preindustrial levels and related global greenhouse gas emission pathways. *Special Report, Intergovernmental Panel on Climate Change*, 175–311.

IPCC. 2022. Contribution of Working Group II to the Sixth Assessment Report of the Intergovernmental Panel on Climate Change. Cambridge University Press. In Press., 1–225.

Jiao, W., L. Wang, and M. F. McCabe. 2021. Multi-sensor remote sensing for drought characterization: Current status, opportunities and a roadmap for the future. *Remote Sensing of Environment* 256:112313.

Jin, S. and T. Zhang. 2016. Terrestrial water storage anomalies associated with drought in southwestern USA from GPS observations. *Surveys in Geophysics* 37:1139–1156.

Jin, S., L. J. Zhang, and B. D. Tapley. 2011. The understanding of length-of-day variations from satellite gravity and laser ranging measurements. *Geophysical Journal International* 184:651–660.

Khaki, M., E. Forootan, M. Kuhn, J. Awange, L. Longuevergne, and Y. Wada. 2018. Efficient basin scale filtering of GRACE satellite products. *Remote Sensing of Environment* 204:76–93.

Khorrami, B. and O. Gunduz. 2021. An enhanced water storage deficit index (EWSDI) for drought detection using GRACE gravity estimates. *Journal of Hydrology*., 603, 126812.

Kumar, S. V., B. F. Zaitchik, C. D. Peters-Lidard, M. Rodell, R. Reichle, B. Li, M. Jasinski, D. Mocko, A. Getirana, G. De Lannoy, M. H. Cosh, C. R. Hain, M. Anderson, K. R. Arsenault, Y. Xia, and M. Ek. 2016. Assimilation of gridded GRACE terrestrial water storage estimates in the North American land data assimilation system. *Journal of Hydrometeorology* 17:1951–1972.

Leblanc, M. J., P. Tregoning, G. Ramillien, S.O. Tweed, and A. Fakes. 2009. Basin-scale, integrated observations of the early 21st century multiyear drought in southeast Australia. *Water Resources Research* 45:1–4.

Li, B., M. Rodell, S. Kumar, H. K. Beaudoing, A. Getirana, B. F. Zaitchik, L. G. de Goncalves, C. Cossetin, S. Bhanja, A. Mukherjee, S. Tian, N. Tangdamrongsub, D. Long, J. Nanteza, J. Lee, F. Policelli, I. B. Goni, D. Daira, M. Bila, G. Lannoy, D. Mocko, S. Steele-Dunne, H. Save, S. Bettaetdpur. 2019. Global GRACE data assimilation for groundwater and drought monitoring: Advances and challenges. *Water Resources Research* 55:7564–7586.

Liu, X., X. Feng, P. Ciais, B. Fu, B. Hu, and Z. Sun. 2020. GRACE satellite-based drought index indicating increased impact of drought over major basins in China during 2002–2017. *Agricultural and Forest Meteorology* 291:108057.

Lopez, T., A. Al Bitar, S. Biancamaria, A. Güntner, and A. Jäggi. 2020. On the use of satellite remote sensing to detect floods and droughts at large scales. *Surveys in Geophysics* 41:1461–1487.

Masih, I., S. Maskey, F.E.F. Mussá, and P. Trambauer. 2014. A review of droughts on the African continent: A geospatial and long-term perspective. *Hydrology and Earth System Sciences* 18:3635–3649.

Mekonnen, K., A. M. Melesse, and T. A. Woldesenbet. 2022. How suitable are satellite rainfall estimates in simulating high flows and actual evapotranspiration in MelkaKunitre catchment, Upper Awash Basin, Ethiopia? *Science of the Total Environment* 806:150443.

Mgquba, S. K. and S. Majozi. 2020. Climate change and its impacts on hydro-politics in transboundary basins: A case study of the orange-senqu river basin. *Journal of Water and Climate Change* 11:150–165.

Modanesi, S., C. Massari, S. Camici, L. Brocca, and G. Amarnath. 2020. Do satellite surface soil moisture observations better retain information about crop-yield variability in drought conditions? *Water Resources Research* 56:e2019WR025855.

Müller Schmied, H., D. Caceres, S. Eisner, M. Flörke, C. Herbert, C. Niemann, T. Asali Peiris, E. Popat, F. Theodor Portmann, R. Reinecke, M. Schumacher, S. Shadkam, C. E. Telteu, T. Trautmann, and P. Döll. 2021. The global water resources and use model WaterGAP v2.2d: Model description and evaluation. *Geoscientific Model Development* 14:1037–1079.

Munday, C. and R. Washington. 2019. Controls on the diversity in climate model projections of early summer drying over southern Africa. *Journal of Climate* 32:3707–3725.

Ndehedehe, C. E.; J. L. Awange, M. Kuhn, N. O. Agutu, Y. Fukuda. 2017. Climate teleconnections influence on West Africa's terrestrial water storage. *Hydrological Processes*., 31, 3206–3224.

Ndehedehe, C. E., J. L. Awange, N. O. Agutu, and O. Okwuashi. 2018. Changes in hydro-meteorological conditions over tropical West Africa (1980–2015) and links to global climate. *Global and Planetary Change* 162:321–341.

Ndehedehe, C. E.; R. O. Anyah, D. Alsdorf, N. O. Agutu, V. G. Ferreira. 2019. Modelling the impacts of global multi-scale climatic drivers on hydro-climatic extremes (1901–2014) over the Congo basin. *Science of The Total Environment*., 651, 1569–1587.

Ndehedehe, C. E., V. G. Ferreira, A. O. Onojeghuo, N. O. Agutu, E. Emengini, and A. Getirana. 2020. Influence of global climate on freshwater changes in Africa's largest endorheic basin using multi-scaled indicators. *Science of the Total Environment* 737:139643.

Ni, S., J. Chen, C. R. Wilson, J. Li, X. Hu, and R. Fu. 2018. global terrestrial water storage changes and connections to ENSO events. *Surveys in Geophysics* 39:1–22.

Nigatu, Z. M., D. Fan, W. You, and A. M. Melesse. 2021. Hydroclimatic extremes evaluation using GRACE/GRACE-FO and multidecadal climatic variables over the Nile River Basin. *Remote Sensing* 13:651.

Oguntunde, P. G.; G. Lischeid, B. J. Abiodun. 2018. Impacts of climate variability and change on drought characteristics in the Niger River Basin, West Africa. *Stochastic Environmental Research and Risk Assessment*., 32, 1017–1034.

Omer, A., M. Zhuguo, Z. Zheng, and F. Saleem. 2020. Natural and anthropogenic influences on the recent droughts in Yellow River Basin, China. *Science of the Total Environment* 704:135428.

Papa, F., J. F. Crétaux, M. Grippa, E. Robert, M. Trigg, R. M. Tshimanga, B. Kitambo, A. Paris, A. Carr, A. S. Fleischmann, M. de Fleury, P. G. Gbetkom, B. Calmettes, and S. Calmant. 2022. Water resources in Africa under global change: Monitoring surface waters from space. *Surveys in Geophysics* 4:1–51.

Running, S., Q. Mu, M. Zhao, and A. Moreno. 2017. MOD16A2—MODIS/Terra Net Evapotranspiration 8-Day L4 Global 500m SIN Grid V006 [Data set]. *NASA EOSDIS Land Processes DAAC* 1.5:34.

Sarfo, I., B. Shuoben, L. Beibei, S.O.Y. Amankwah, E. Yeboah, J. E. Koku, E. K. Nunoo, and C. Kwang. 2022. Spatiotemporal development of land use systems, influences and climate variability in southwestern Ghana (1970–2020). *Environment, Development and Sustainability* 24:9851–9883.

Satish Kumar, K.; E. Venkata Rathnam, V. Sridhar. 2021. Tracking seasonal and monthly drought with GRACE-based terrestrial water storage assessments over major river basins in South India. *Science of The Total Environment*., 763, 142994.

Schlosser, C. A., K. Strzepek, X. Gao, C. Fant, É. Blanc, S. Paltsev, H. Jacoby, J. Reilly, and A. Gueneau. 2014: The future of global water stress: An integrated assessment. *Earth's Future* 2:341–361.

Sun, Z., X. Zhu, Y. Pan, J. Zhang, and X. Liu. 2018. Drought evaluation using the GRACE terrestrial water storage deficit over the Yangtze River Basin, China. *Science of the Total Environment* 634:727–738.

Thomas, A. C.; J. T. Reager, J. S. Famiglietti, M. Rodell. 2014. A GRACE-based water storage deficit approach for hydrological drought characterization. *Geophysical Research Letters*., 41, 1537–1545.

United Nations Environment Programme. 2010. Africa water atlas, 1, 1–336.

Vicente-Serrano, S. M., S. Beguería, L. Gimeno, L. Eklundh, G. Giuliani, D. Weston, A. El Kenawy, J. I. López-Moreno, R. Nieto, T. Ayenew, D. Konte, J. Ardö, and G.G.S. Pegram. 2012. Challenges for drought mitigation in Africa: The potential use of geospatial data and drought information systems. *Applied Geography* 34:471–486.

Wang, J., Y. Chen, Z. Wang, and P. Shang. 2020. Drought evaluation over Yangtze River basin based on weighted water storage deficit. *Journal of Hydrology* 591:125283.

Wang, L., J. Wang, L. Wang, L. Zhu, and X. Li. 2022. Terrestrial water storage regime and its change in the endorheic Tibetan Plateau. *Science of the Total Environment* 815:152729.

Wells, N., S. Goddard, and M. J. Hayes. 2004. A self-calibrating Palmer Drought Severity Index. *Journal of Climate* 17:2335–2351.

West, H., N. Quinn, and M. Horswell. 2019. Remote sensing for drought monitoring and impact assessment: Progress, past challenges and future opportunities. *Remote Sensing of Environment* 232:111291.

Wu, T., W. Zheng, W. Yin, and H. Zhang. 2021. Spatiotemporal characteristics of drought and driving factors based on the GRACE-derived total storage deficit index: A case study in Southwest China. *Remote Sensing* 13:79.

Yang, P., J. Xia, C. Zhan, Y. Qiao, and Y. Wang. 2017. Monitoring the spatio-temporal changes of terrestrial water storage using GRACE data in the Tarim River basin between 2002 and 2015. *Science of the Total Environment* 595:218–228.

Zargar, A., R. Sadiq, B. Naser, and F. I. Khan. 2011. A review of drought indices. *Environmental Reviews* 19:333–349.

Zhang, B., E. Zhang, L. Liu, S. A. Khan, T. van Dam, Y. Yao, M. Bevis, and V. Helm. 2018. Geodetic measurements reveal short-term changes of glacial mass near Jakobshavn Isbræ (Greenland) from 2007 to 2017. *Earth and Planetary Science Letters* 503:216–226.

Zhang, Y., B.I.N. He, L. Guo, and D. Liu. 2019. Differences in response of terrestrial water storage components to precipitation over 168 global river basins. *Journal of Hydrometeorology* 20:1981–1999.